This File contains Supplementary Materials and Methods and 8 Supplementary Figures.

Supplementary Material and Methods

Gene expression profiling analyses. TCGA breast cancer transcriptional profiling data previously analyzed in (1) were downloaded from the TCGA website https://tcga-data.nci.nih.gov/docs/publications/brca_2012/ (file BRCA.exp.547.med.txt, level 3 data freeze from November 2011). Data were processed on Agilent custom 244K whole genome arrays for 522 tumors, 3 metastatic tumors, and 22 tumor-adjacent normal and provided as median centered on 17,184 genes. Genes with a low dynamic range (estimated by standard deviation < 0.5 and max - min expression across samples < 1.5) were filtered out and the expression data were restricted to the 12,459 reliable genes. Clinical information on estrogen receptor (ER) status and progesteron receptor (PR) status were available in the BRCA_Clinical.tar/nationwidechildrens.org_ clinical_patient_public_brca.txt file with several clinical information inconsistencies highlighted in (1). ERBB2 clinical status was assessed as described by integrating immunohistochemistry results with FISH results and copy number calls. Breast cancer intrinsic subtypes were assigned for 514 of the 522 primary tumors based on the PAM50 calls (file BRCA.547.PAM50.SigClust.Subtypes.txt) (1, 2) as Basal (98 samples out of which 82 were triple negative tumors), Her2 (58 samples), Luminal A (231 samples) and Luminal B (127 samples). Amplification status for the chr1q32.1 region harboring IKKε as estimated by GISTIC (3) was available for 498 primary tumors.

The IKKε high/low status for individual tumors was evaluated based on the z-scores of IKKε expression and the absolute cutoff threshold 1. In statistics, the z-score is the (signed) number of standard deviations an observation is above the mean. The z-scores of IKKε expression were

computed by subtracting from the gene expression for each sample the average gene expression across all samples and by dividing the result to the standard deviation of gene expression across samples. High IKKε status was assigned to samples with z-scores above 1.

TNBC subtypes used for unsupervised clustering were identified within the 82 basal TCGA samples with negative ER and negative PR status by applying the ssGSEA method (see below) for six TNBC subtype signatures identified by Lehman et al (4). In their study Lehman et al analyzed gene expression profiles for 587 TNBC samples from 21 breast cancer data sets and identified six TNBC subtypes displaying unique gene expression signatures and ontologies, including 2 basal-like (BL1 and BL2), an immunomodulatory (IM), a mesenchymal (M), a mesenchymal stem–like (MSL), and a luminal androgen receptor (LAR) subtype. The gene signatures consisting of top 300 genes up-regulated and top 300 genes down regulated in each of the six TNBC subtypes versus all others were provided by Supplementary Table S3 in Lehman et al. The B-cell cluster signature reflects lymphocytic infiltration and was derived from Iglesia et al (5). Correlation of IKKε mRNA expression with TP53 mutational status (present or absent) within the TCGA dataset was analyzed by two sample t-test in all tumors and in the TNBC subset. The relationship between IKKε levels and Miller-Payne response to neoadjuvant cisplatin (6) was also measured by t-test comparison of poor (0-2) and good (3-5) responders.

The single sample GSEA (ssGSEA) Method. The ssGSEA method (7) and implemented in GenePattern v3.6.1 (8) provides for each individual tumor sample an enrichment score (ES) with respect to a priori defined gene set signatures. The enrichment score provides evidence for the coordinate up- or down-regulation of a gene set's members within individual samples. In

ssGSEA the genes for each individual sample are ranked based on their expression intensity by applying the RankNormalize method implemented in GenePattern (8). ES is calculated as a running sum statistic by walking down across the ranked list of genes, increasing the sum when encountering genes in the gene set and decreasing it when encountering genes not in the gene set. A positive ES denotes a significant overlap of the signature gene set with groups of genes at the top of the ranked list, while a negative ES denotes a significant overlap of the signature gene set with groups of genes at the bottom of the ranked list.

The IL-1 and IL-6 signatures were derived from the transcriptome profile of cultured human macrophages stimulated for 4 h with interleukin 1 (IL-1) and interleukin 6 (IL-6) (9) derived from the NCBI/Genbank GEO database (series entry GSE8515). The IL-1 signature was defined based on the collection of 127 probe sets strongly activated by IL-1 only (cluster A) along with the collection of 43 probe sets activated by both IL-1 and IL-6 (cluster C) (9). TNF, IFN-γ, and IFN-2α signatures were generated from stimulated monocytes (10) based on GEO dataset GSE38351. Correlation with IKKε mRNA expression was assessed using the normalized mutual information statistic as described in (11).

The IL-1 high/low status for individual tumors was evaluated based on the z-scores of enrichment with the IL-1 signature and the absolute cutoff threshold 1. ES scores for IL-1 signature enrichment were evaluated for each primary tumor sample by applying the ssGSEA method described above. The z-scores of IL-1 enrichment were then computed by subtracting from the ES value of each sample the average of the ES values across all samples and by

dividing the result to their standard deviation. High IL-1 status was assigned to samples with enrichment z-scores above 1.

Cell Culture. All breast cancer cell lines and 293T cells were obtained from ATCC and cultured in the recommended media for each cell line with supplements as per ATCC guidelines. Immortalized human mammary epithelial cells (HMLE) isogenic for IKKε expression (myristolated-Flag-IKKε or vector control) were cultured as described (12). For suspension culture of triple negative breast cancer cell lines, cells were plated onto ultra low attachment plates (from Corning Costar) for 48 h in their respective medium with or without IL-1β (25 ng/ml) and CYT387.

3D culture was performed as described using a novel microfluidic device (13). In brief, the device consists of a central gel region surrounded by two channels on either side formed by bonding a coverslip to a patterned polydimethylsiloxane (PDMS) substrate. MDA-MB-468 breast cancer cell spheroids obtained following 10-14 d suspension culture were embedded in collagen matrigel in the central gel region. One channel was used to infuse media and the other for stimulation of spheroid dispersal by addition of growth factor (EGF 20 ng/ml) or cytokines (CCL5 and IL-6 each at 20 ng/ml). Cell dispersal was monitored over time by phase-contrast imaging after growth factor/cytokine addition with or without CYT387 treatment. For angiogenesis experiments, HUVECs were seeded in the central channel of the 3 chamber angiogenesis device, surrounded by collagen on either side. Control media was infused through one channel, while 293T cells transfected with IKKε x 24 h were seeded in the opposing channel,

or CCL5/IL-6 (20 ng/ml each) were added directly to media in this channel. HUVEC cell migration was observed into collagen by phase-contrast imaging and distance was quantified after 24 h. For MEK inhibitor experiments, GSK1120212 was added to CCL5/IL-6 at the indicated concentrations.

Inhibitors, Growth Factors/Cytokines, and ELISA. CYT387 and Ruxolitinib were purchased from Shanghai Haoyuan Chemexpress Co. Ltd. EGF (#4127) was from Sigma, IL-1β (#201-LB), IL-6 (#206-IL), and CCL5 (#278-RN) were obtained from R&D. ELISA kits for IL-6 (D6050) and CCL5 (DRN00B) levels were from R&D and were performed according to the manufacturer's instructions. Media was collected following transfection of 293T cells with EGFP or IKKε +/- CYT387 (5μM) starting 12 h post-transfection, or following stimulation of the TNBC lines with IL-1β (25 ng/ml) for 24h +/- CYT387 (5μM). Proteome Profiler^{TM} Human Cytokine Array (ARY005) was purchased from R&D and treated with media from 293T cells transfected with EGFP as a control, or IKKε +/- CYT387 (5μM) starting 12 h post-transfection. Media was collected 24 h after transfection, the blot was performed according to the manufacturer's instructions and imaged using standard ECL-based detection and autoradiography. Proteome Profiler^{TM} Human Phospho-kinase Array (ARY003B) was treated with lysates from the same 293T cells, processed, and imaged by ECL-based detection and autoradiography according to the manufacturer's instructions.

Antibodies and Immunoblotting. Immunoblotting was performed according to a standard protocol (14). Anti-STAT3 (#9132), Y705 pSTAT3 (#9145), STAT5 (#9358), Y694 pSTAT5

(#4322), p105 (#4717), S933 p-p105 (#4806), IKKα (#2682), IKKβ (#2370), and T180/Y182 p-p38 (#4511) were from Cell Signaling Technologies. β-Actin antibody was from Santa Cruz Biotechnology (#sc-47778 HRP). IKKε antibody was from Sigma (#I4907). Secondary antibodies were from Bio-Rad. Blots were developed using standard ECL-based detection and autoradiography.

Transfection, Lentiviral Infection, Constructs. 293T cells were transfected using Fugene 6 reagent (#11815091001, Roche) according to the manufacterer's instructions with 1 μg of plasmid. Lentiviral infection of shRNAs or ORFs was performed as described (7, 15). For selection of virally infected cells, 1-2 μg/ml of Puromycin (pLKO.1) or 5-10 μg/ml of Blasticidin (pLX304) was used 24 h post infection. pLKO.1 shRNA constructs were obtained from the Broad Institute TRC (http://www.broadinstitute.org/rnai/trc) with the following sequences:

shGFP TRCN0000072181: 5' ACAACAGCCACAACGTCTATA 3'
shIKKε-1 TRCN0000010036: 5' TGGGCAGGAGCTAATGTTTCG 3'
shIKKε-2 TRCN0000010027: 5' GAGCATTGGAGTGACCTTGTA 3'

pLX304-GFP, pLX304-IKKε-WT, and pLX304-IKKε-K38A constructs were used for transient transfection of 293T cells. MDA-MB-468-IKKe-Y88C cells were generated by stable transduction of MDA-MB-468 cells by lentiviral infection with pLX304-IKKe-Y88C using blasticidin selection, followed by treatment in CYT387 (2.5 μM) for 3 weeks.

Quantitative Real-Time PCR. RNA was extracted from transfected 293T cells or snap-frozen xenograft tumors using PerfectPure RNA Kit (5 PRIME). Reverse transcription of 1 μg RNA

samples was performed using SuperScript® III First-Strand Synthesis SuperMix (Invitrogen). Quantitative real-time PCR was conducted using LightCycler® 480 SYBR Green I Master (Roche) and Light Cycler 480 II real-time PCR system (Roche). Values were normalized to 36B4. The sequences of the primers used for RT-PCR are:

CCL5: FWD 5'CGCTGTCATCCTCATTGCTA3', REV 5'GAGCACTTGCCACTGGTGTA3'
IL6: FWD 5'TCAATGAGGAGACTTGCCTG3', REV 5'TCATCTGCACAGCTCTGGCT3'
IKKε: FWD 5'ATTACAACACTGCCAAGGGC3', REV 5'AGCACCTCCATGACCCAGTG3'
36B4: FWD 5'GCAATGTTGCCAGTGTCTGT3', REV 5'GCCTTGACCTTTTCAGCAAG3'

Animal Studies. MDA-MB-468 xenografts were established following subcutaneous injection of 1X10^6 cells into nude mice. WHIM patient derived xenografts were cultured as described (16, 17). Mice with established tumors were treated by daily oral gavage with vehicle control or CYT387 dissolved in N-Methyl-2-pyrrolidone (Sigma-Aldrich) at 100 mg/mL and mixed with a methylcellulose/tween vehicle (0.5% methylcellulose (Sigma-Aldrich) and 0.4% polysorbate-80 (Tween-80) (Sigma-Aldrich) in sterile water for daily oral gavage dose of 100 mg/kg. Tumor area measurements were obtained in a blinded fashion, and tumor volume was calculated using the formula $((\text{width})^2 \times \text{length})/2$.

For short term pharmacodynamics studies mice were treated for 3 d to achieve steady state inhibition and tumors were harvested 6 h after the final dose of drug. Tumors were isolated and snap frozen for qRT-PCR or immunoblotting, or formalin fixed for immunohistochemistry (IHC). IHC staining was performed on FFPE tissue sectioned at 5μm thickness. Slides were deparaffinized, rehydrated and treated with 3% H2O2 in PBS. Antigen retrieval was achieved by microwaving in a pressure cooker for 15 min in Antigen Retrieval Citra Solution (BioGenex,

HK086-9K). Sections were incubated with Peroxidase Blocking Reagent (Dako, S2001) for 15 min, and Protein Block (Dako, X0909) for 15 min. Anti-pSTAT3 (Cell Signaling Technology, 9131; 1:70 dilution) was applied for 16 h at 4°C, followed by EnVision™+/HRP, Rabbit (Dako, K4003), diaminobenzidine (Dako, K3468), and hematoxylin counterstain. pSTAT3 expression was evaluated by two blinded pathologists (Y.I. and Z.R.Q.).

Histopathologic analysis. A total of 11 formalin-fixed, paraffin-embedded WHIM21 xenograft tumors treated with vehicle control (n = 3), 50mg/kg/d CYT387 (n = 2), 2.5mg/kg/d GSK112012 (n = 2), or CYT387 andGSK112012 in combination (n = 4), respectively. Pathology review of the H&E staining and the subsequent immunohistochemical stains were conducted manually by a trained pathologist in the Dana-Farber Cancer Institute Molecular Pathology Core.

Immunohistochemical staining of Ki67, CD31 and ERG were performed on 4-µm sections of the FFPE WHIM21 xenograft tissue; using the Bond Refine Detection System following the manufacturer's protocols on the Leica Bond III automated immunostainer. The sections were automatically deparaffinized, antigen retrieval was performed with Bond Epitope Retrieval Solution 1 (HIER1, pH 6.0) and processed for 20 min. The slides were incubated with the antibody against Ki67 (VP-K451, Rabbit polyclonal, Vector) at a dilution of 1:1500 for 60 min, CD31 (Rabbit polyclonal, ab28364, Abcam) at a dilution of 1:50 for 20 min and ERG (Rabbit monoclonal, #2805-1, Epitomics) at a dilution of 1:200 for 60 min, respectively. The sections were then treated according to the streptavidin–biotin–peroxidase complex method (Bond Polymer Refine Detection, Leica Microsystems) with diaminobenzidine (DAB) as a chromogen and counterstained with hematoxylin. Tonsil tissue was used as a positive control for Ki67 and

CD31; Prostate cancer tissue was used as positive controls for ERG. Omission of the primary antibody was utilized as a negative control.

The Ki67 labeling index scoring and microvessel density (MVD) estimation were visually performed by histopathology using an Olympus CX41 light microscope. High resolution, high magnification 40x images were taken with the Image Capture software (Company, version X). For each individual case, the region of most intense staining (or "hot spot") was identified with 4x and 10x object lenses. Ki-67 score was assessed in a minimum of 10 consecutive High Power Fields (HPFs, 400x) in the representative "hot spot" area. The Ki67 labeling index was calculated as the percentage of positively stained tumor cells relative to total tumor cells. To evaluate MVD, slides stained with anti-CD31 antibody were examined. Single endothelial cell or clusters of endothelial cells positive for CD31 were considered as a vessel; Vessels with muscular walls were not counted. For each case, the number of microvessels was counted in a minimum of 6 consecutive HPFs (HPF size 0.95 mm^2) in the "hot spot" area. MVD was then estimated as a mean of the number of microvessels per square millimeter (microvessel/mm^2).

Supplementary Figures

Supplemental Figure 1. IKKε expression correlates with IL-1 associated immune signaling in TNBC. (**A**) Relationship between IKKε mRNA levels and expression of several different cytokine gene signatures across breast cancers in the TCGA dataset. The degree of cytokine signature expression were measured using single sample GSEA (ssGSEA), NMI = normalized mutual information statistic. **p<0.001 (**B**) Correlation between *IKKε* mRNA and IL-1 signature expression in TNBC, $HER2^+$ or Luminal breast tumors. Odds ratios were calculated by two

tailed Fisher tests. The high/low status for IKKε was estimated based on z-scores of *IKKε* expression across samples. The high/low status for IL-1 was estimated based on z-scores for ssGSEA enrichment of the IL-1 signature across samples. (**C**) Unsupervised clustering of *IKKε* mRNA and IL-1 signature expression with other previously described TNBC subtypes and with a previously described lymphocyte infiltration signature. Yellow bar indicates the association between *IKKε* mRNA, IL-1 signature, immunomodulatory subtype (NMI = 0.28) and B-cell cluster (NMI = 0.15), **p<0.001, *p<0.02

Supplemental Figure 2. Correlation of IKKε mRNA levels with *TP53* status and response to cisplatin. (**A**) Log2 mRNA expression of IKKε sorted by the presence or absence of TP53 mutation, analyzed by t-test across all tumors (p=0.01) or TNBC subset (p=0.58). (**B**) Log2 mRNA expression of IKKε sorted by Miller-Payne response to neoadjuvant cisplatin in a cohort of TNBC patients. No significant difference was observed by t-test (p = 0.74).

Supplemental Figure 3. Inhibition of IKKε alone is insufficient to disrupt cytokine expression TNBC cells. (**A**) MDA-MB468 cells were infected with a control shRNA or 2 different IKKε specific shRNAs and stimulated with IL-1β for 4 h. CCL5 or IL-6 levels were measured by ELISA. Mean and SD of duplicate samples shown. (**B**) Immunoblot of IKKε and β-actin levels in MDA-MB468 cells following control or IKKε shRNA expression.

Supplemental Figure 4. CYT387 treatment inhibits migration and anchorage independent proliferation of TNBC cells. (**A**) Phase contrast images of MDA-MB-468 spheroids in microfluidic 3D culture stimulated to proliferate and migrate with EGF (20 ng/ml). Spheroids were treated with DMSO as a control or CYT387 at the indicated concentrations. Representative spheroid dispersal at 48 h shown (20x). (**B**) Phase contrast images (10x) of multiple other TNBC

cell lines cultured in suspension using ultra-low cluster plates and stimulated to proliferate with IL-1β (25 ng/ml) in the presence of DMSO or 5 μM CYT387.

Supplemental Figure 5. CYT387 treatment disrupts IKKε-associated STAT and NF-κB signaling. (**A**) Proteomics array measuring the phosphorylation status of 45 different proteins involved in signal transduction 24 h following control EGFP expression or IKKε with 12 h DMSO or CYT387 (5 μM) pretreatment. Highlighted are STAT family members as well as p38α, which were induced by IKKε and suppressed by CYT387 treatment. (**B**) Levels of Y694 pSTAT5, total STAT5, and β-actin following EGFP or IKKε overexpression in 293T cells and treatment with DMSO, 5 μM Ruxolitinib or 5 μM CYT387. (**C**) Levels of T180/Y182 p-p38 and β-actin following EGFP or IKKε overexpression in 293T cells and treatment with DMSO, Ruxolitinib or CYT387. (**D**) Immunoblot of T180/Y182 p-p38 and β-actin levels in MDA-MB-468 cells treated with DMSO, 5 μM Ruxolitinib or 5 μM CYT387 for the indicated times. (**E**) Levels of S933 p-p105, total p105, and β-actin in the indicated TNBC cell lines following DMSO or 5 μM CYT387 treatment for x 1 h. (**F**) Immunoblot of IKKε, pSTAT3, and β-actin levels in the indicated TNBC cell lines following 24 h, 48 h, or 72 h DMSO or 5 μM CYT387 treatment.

Supplemental Figure 6. Autocrine and paracrine effects of IKKε regulated cytokines. (**A**) ELISA measuring CCL5 or IL-6 levels in HCC1187 or HCC70 cells x 24 h following IL-1β (25 ng/ml) with DMSO as a control or 5 μM CYT387 treatment. Values represent mean and SD of duplicate samples. **(B)** Relative viability of MDA-MB-468 cells in 2D culture by CTG 72 h following 5μM Ruxolitinib or CYT387 treatment, or CYT387 + CCL5, IL-6, CCL5/IL-6, compared with DMSO control. Mean and SEM of triplicate samples shown, ** $p<0.001$ by t-test

for comparison of CYT alone to cytokine addition. (**C**) 293T cells transfected with EGFP, IKKε-WT or IKKε-KD were seeded after 24 hours into the channel as indicated, such that conditioned media diffused towards HUVECs into the central channel (arrows). Phase contrast images (20x) and quantification of migration show that IKKε-WT expressing cells specifically induced HUVEC migration. (**D**) High resolution 40x image of HUVEC cell proliferation during CCL5/IL-6 induced migration (arrows indicate nuclear division).

Supplemental Figure 7. IKKε expression across TNBC PDX tumors and WHIM21 response to therapy**.** (**A**) Relative levels of IKKε mRNA in a WHIM tumor panel, scale levels of normalized expression, white = not tested. Highlighted are WHIM4 and WHIM21 tumors, TNBC WHIM tumor models that showed high level IKKε expression, as well as WHIM12, a TNBC that did not over-express IKKε. (**B**) Change in absolute tumor volume over time from subset of CYT387/GSK1120212 treated mice with high initial tumor burden demonstrating regression of established tumors. (**C**) Representative WHIM21 tumors dissected from vehicle, CYT387, GSK1120212 or CYT387+GSK112012 treated mice after 30 d.

Supplemental Figure 8. Low dose CYT387/GSK1120212 combination therapy in IKKε high versus IKKε low TNBC PDX tumors. (**A**) Spider plot of % change in tumor volume over time in WHIM21 tumors treated with vehicle control, high dose Ruxolitinib (100 mg/kg/d), or low dose CYT387 (10 mg/kg/d) combined with GSK1120212 (2.5 mg/kg/d). Over the course of a 30 day treatment Ruxolitinib treated mice progressed similarly to control treated animals, whereas tumor progression was halted over this time period after just 2 weeks of treatment with low dose CYT387/GSK1120212. (**B**) Spider plot of % change in tumor volume following vehicle (n=15) or low dose CYT387/GSK1120212 treatment (n=15) of WHIM12 PDX tumors, a TNBC model

with low levels of IKKε expression. Tumors also responded to therapy, although less dramatically than WHIM21 tumors, with some mice progressing on treatment.

Supplemental Figure 9. Histologic analysis of WHIM21 treated tumors. (**A-D**) Area of necrosis (indicated by arrows) in control, CYT387, GSK1120212, and CYT+GSK treated tumors. (**E-H**) Ki-67 nuclear stain to assess proliferation in viable tumor cells across each condition. (**I-L**) CD31 stain to used to assess microvascular density in regions of viable tumor following each treatment. (**M-P**) Orthogonal assessment of tumor vascularity using ERG immunohistochemistry.

Supplementary References

1. Koboldt, D.C., Fulton, R.S., McLellan, M.D., Schmidt, H., Kalicki-Veizer, J., McMichael, J.F., Fulton, L.L., Dooling, D.J., Ding, L., Mardis, E.R., et al. 2012. Comprehensive molecular portraits of human breast tumours. *Nature* 490:61-70.

2. Parker, J.S., Mullins, M., Cheang, M.C., Leung, S., Voduc, D., Vickery, T., Davies, S., Fauron, C., He, X., Hu, Z., et al. 2009. Supervised risk predictor of breast cancer based on intrinsic subtypes. *J Clin Oncol* 27:1160-1167.

3. Mermel, C.H., Schumacher, S.E., Hill, B., Meyerson, M.L., Beroukhim, R., and Getz, G. 2011. GISTIC2.0 facilitates sensitive and confident localization of the targets of focal somatic copy-number alteration in human cancers. *Genome Biol* 12:R41.

4. Lehmann, B.D., Bauer, J.A., Chen, X., Sanders, M.E., Chakravarthy, A.B., Shyr, Y., and Pietenpol, J.A. 2011. Identification of human triple-negative breast cancer subtypes and preclinical models for selection of targeted therapies. *J Clin Invest* 121:2750-2767.

5. Iglesia, M.D., Vincent, B.G., Parker, J.S., Hoadley, K.A., Carey, L.A., Perou, C.M., and Serody, J.S. 2014. Prognostic B-cell Signatures Using mRNA-Seq in Patients with Subtype-Specific Breast and Ovarian Cancer. *Clin Cancer Res* 20:3818-3829.

6. Silver, D.P., Richardson, A.L., Eklund, A.C., Wang, Z.C., Szallasi, Z., Li, Q., Juul, N., Leong, C.O., Calogrias, D., Buraimoh, A., et al. 2010. Efficacy of neoadjuvant Cisplatin in triple-negative breast cancer. *J Clin Oncol* 28:1145-1153.

7. Barbie, D.A., Tamayo, P., Boehm, J.S., Kim, S.Y., Moody, S.E., Dunn, I.F., Schinzel, A.C., Sandy, P., Meylan, E., Scholl, C., et al. 2009. Systematic RNA interference reveals that oncogenic KRAS-driven cancers require TBK1. *Nature* 462:108-112.

8. Reich, M., Liefeld, T., Gould, J., Lerner, J., Tamayo, P., and Mesirov, J.P. 2006. GenePattern 2.0. *Nat Genet* 38:500-501.

9. Jura, J., Wegrzyn, P., Korostynski, M., Guzik, K., Oczko-Wojciechowska, M., Jarzab, M., Kowalska, M., Piechota, M., Przewlocki, R., and Koj, A. 2008. Identification of interleukin-1 and interleukin-6-responsive genes in human monocyte-derived macrophages using microarrays. *Biochim Biophys Acta* 1779:383-389.

10. Smiljanovic, B., Grun, J.R., Biesen, R., Schulte-Wrede, U., Baumgrass, R., Stuhlmuller, B., Maslinski, W., Hiepe, F., Burmester, G.R., Radbruch, A., et al. 2012. The multifaceted balance of TNF-alpha and type I/II interferon responses in SLE and RA: how monocytes manage the impact of cytokines. *J Mol Med (Berl)* 90:1295-1309.

11. Abazeed, M.E., Adams, D.J., Hurov, K.E., Tamayo, P., Creighton, C.J., Sonkin, D., Giacomelli, A.O., Du, C., Fries, D.F., Wong, K.K., et al. 2013. Integrative radiogenomic profiling of squamous cell lung cancer. *Cancer Res* 73:6289-6298.

12. Boehm, J.S., Zhao, J.J., Yao, J., Kim, S.Y., Firestein, R., Dunn, I.F., Sjostrom, S.K., Garraway, L.A., Weremowicz, S., Richardson, A.L., et al. 2007. Integrative genomic approaches identify IKBKE as a breast cancer oncogene. *Cell* 129:1065-1079.

13. Aref, A.R., Huang, R.Y., Yu, W., Chua, K.N., Sun, W., Tu, T.Y., Bai, J., Sim, W.J., Zervantonakis, I.K., Thiery, J.P., et al. 2013. Screening therapeutic EMT blocking agents in a three-dimensional microenvironment. *Integr Biol (Camb)* 5:381-389.

14. Barbie, T.U., Barbie, D.A., MacLaughlin, D.T., Maheswaran, S., and Donahoe, P.K. 2003. Mullerian Inhibiting Substance inhibits cervical cancer cell growth via a pathway involving p130 and p107. *Proc Natl Acad Sci U S A* 100:15601-15606.

15. Johannessen, C.M., Boehm, J.S., Kim, S.Y., Thomas, S.R., Wardwell, L., Johnson, L.A., Emery, C.M., Stransky, N., Cogdill, A.P., Barretina, J., et al. 2010. COT drives resistance to RAF inhibition through MAP kinase pathway reactivation. *Nature* 468:968-972.

16. Li, S., Shen, D., Shao, J., Crowder, R., Liu, W., Prat, A., He, X., Liu, S., Hoog, J., Lu, C., et al. 2013. Endocrine-therapy-resistant ESR1 variants revealed by genomic characterization of breast-cancer-derived xenografts. *Cell Rep* 4:1116-1130.

17. Ma, C.X., Cai, S., Li, S., Ryan, C.E., Guo, Z., Schaiff, W.T., Lin, L., Hoog, J., Goiffon, R.J., Prat, A., et al. 2012. Targeting Chk1 in p53-deficient triple-negative breast cancer is therapeutically beneficial in human-in-mouse tumor models. *J Clin Invest* 122:1541-1552.

A

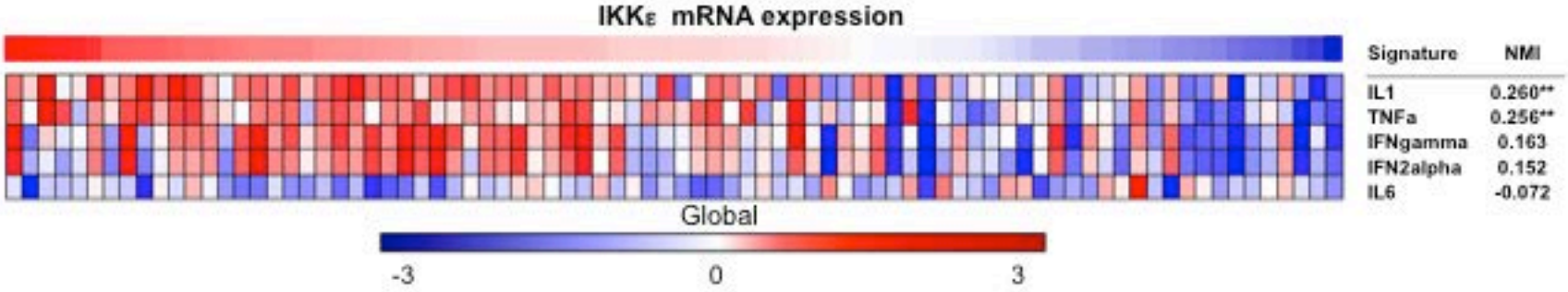

B

	TNBC	Other	Basal non-TBNC	Other	HER2	Other	Lum A	Other	Lum B	Other
IKKε ↑ & IL1 ↑	18	15	3	30	1	32	1	32	10	23
Other	64	417	13	468	57	424	230	251	117	364
	OR = 7.76 p = 1.15e-07		**OR = 3.58** p =0.07		**OR = 0.23** p = 0.15		**OR = 0.03** p = 5.06e-08		**OR = 1.35** p = 0.41	

C

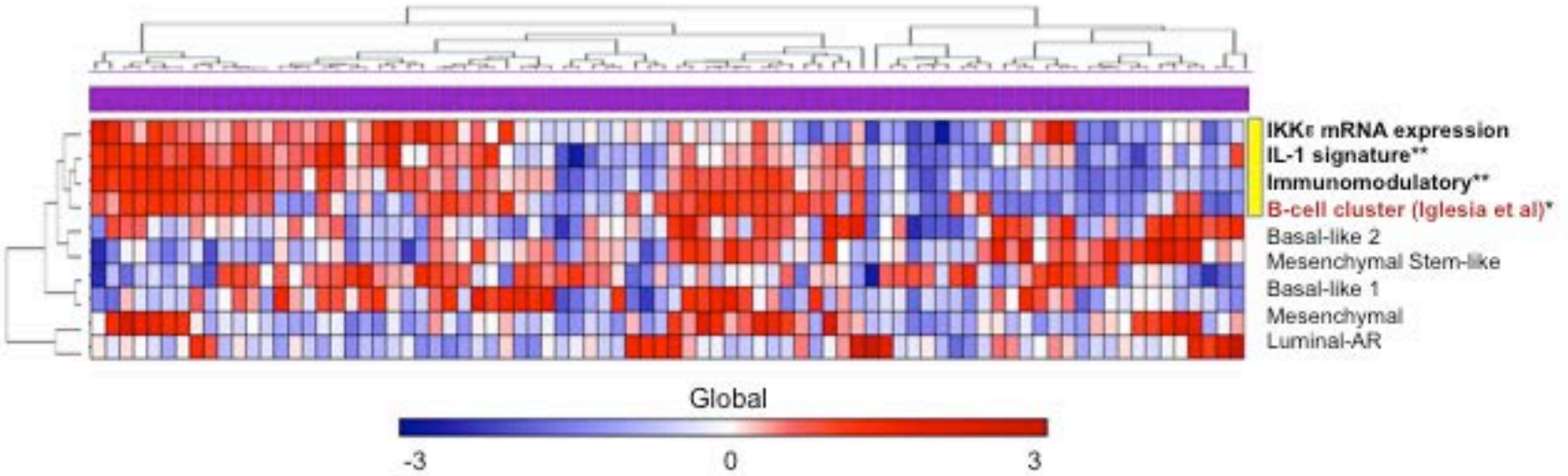

Figure S1

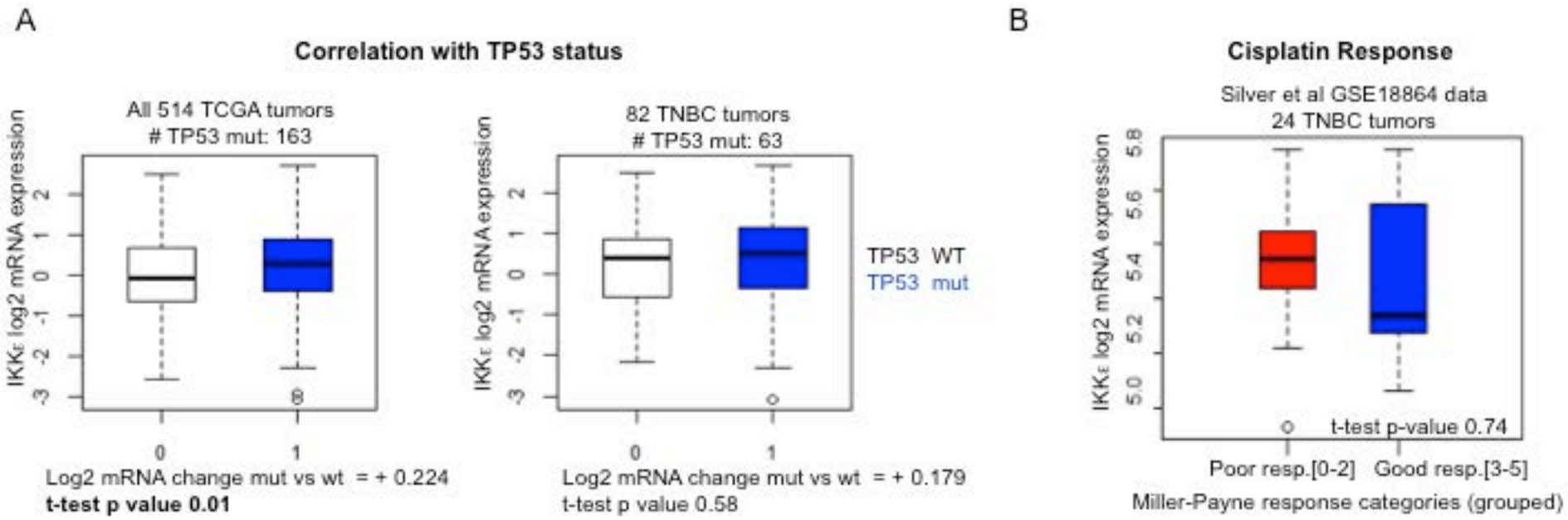
A
Correlation with TP53 status
All 514 TCGA tumors
TP53 mut: 163
IKKε log2 mRNA expression
Log2 mRNA change mut vs wt = + 0.224
t-test p value 0.01
82 TNBC tumors
TP53 mut: 63
Log2 mRNA change mut vs wt = + 0.179
t-test p value 0.58
TP53 WT
TP53 mut
B
Cisplatin Response
Silver et al GSE18864 data
24 TNBC tumors
t-test p-value 0.74
Poor resp.[0-2]
Good resp.[3-5]
Miller-Payne response categories (grouped)

Figure S2

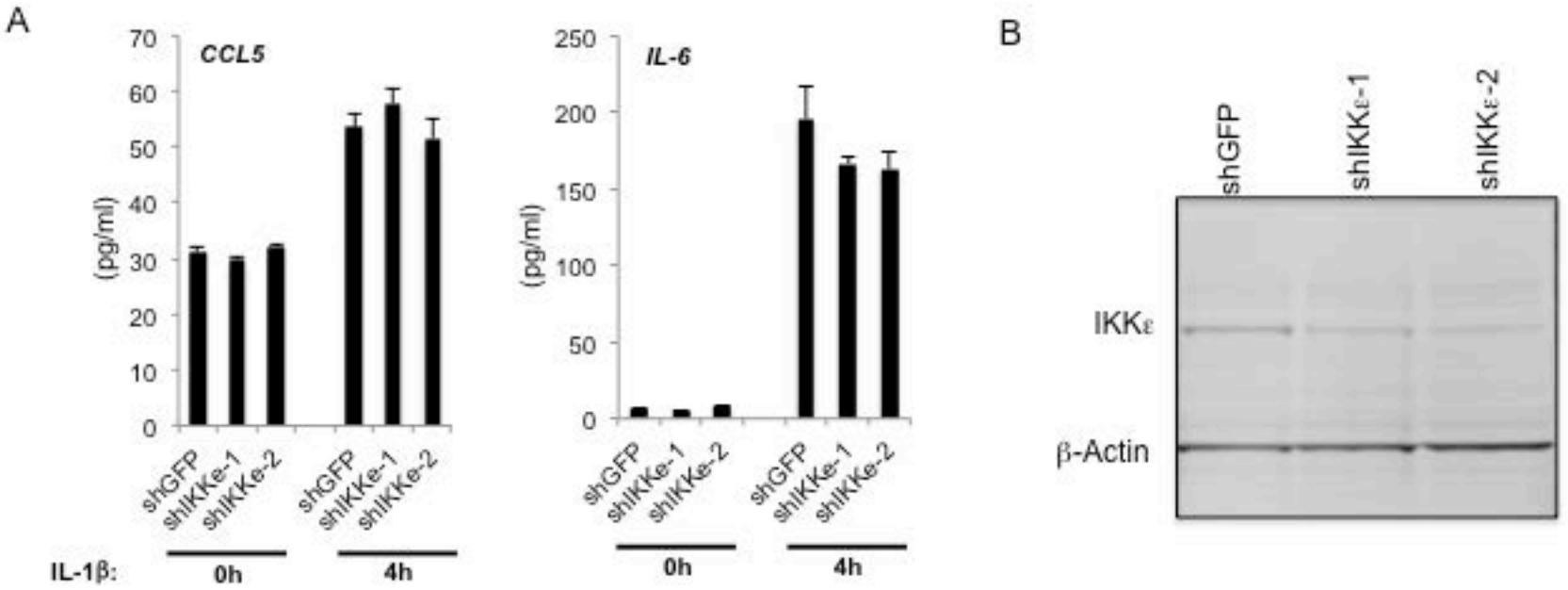
MDA-MB-468 Cells
A
CCL5
(pg/ml)
70
60
50
40
30
20
10
0
shGFP
shIKKε-1
shIKKε-2
IL-1β:
0h
4h
IL-6
250
200
150
100
50
B
shGFP
shIKKε-1
shIKKε-2
IKKε
β-Actin

Figure S3

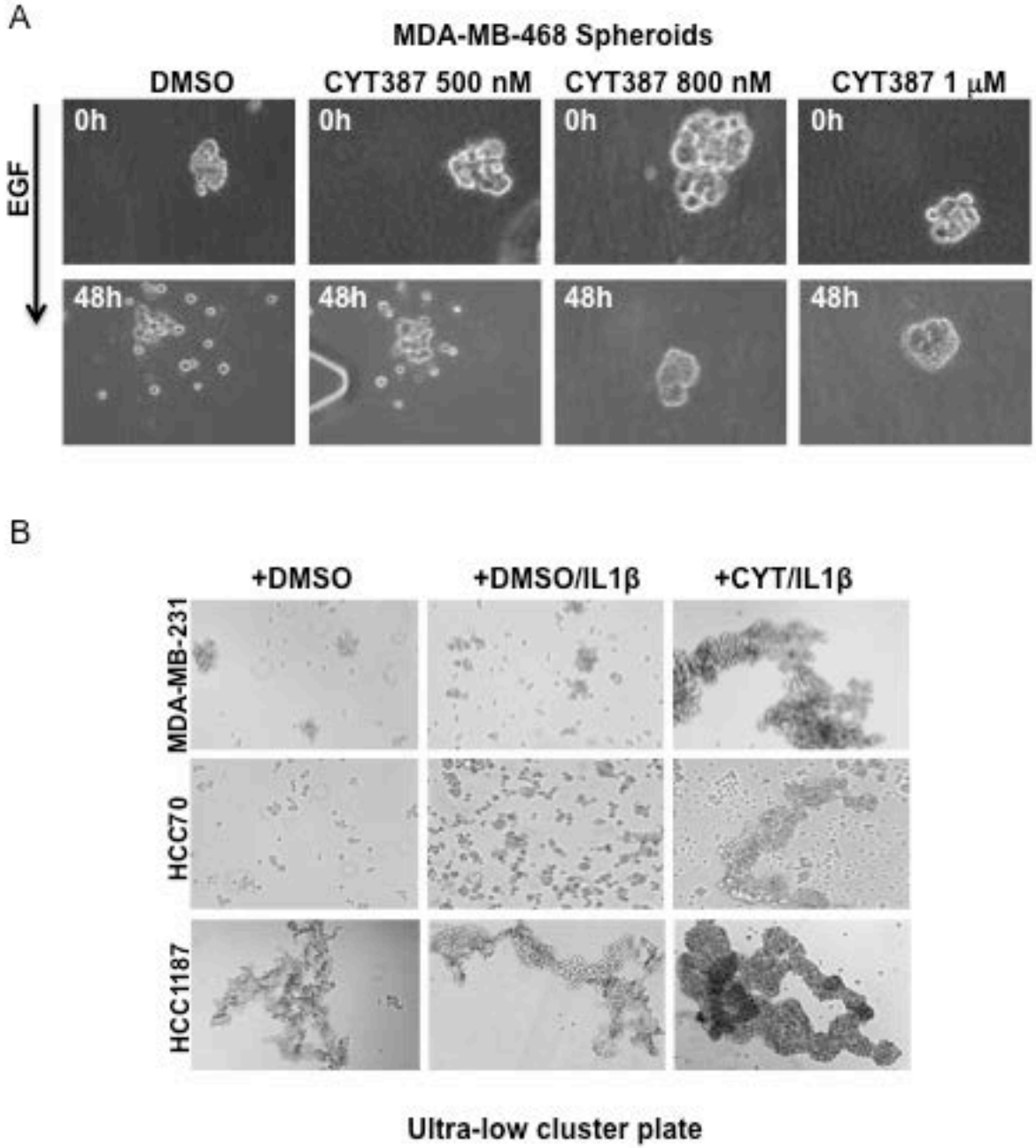
A
MDA-MB-468 Spheroids
DMSO
CYT387 500 nM
CYT387 800 nM
CYT387 1 μM
EGF
0h
48h
B
+DMSO
+DMSO/IL1β
+CYT/IL1β
MDA-MB-231
HCC70
HCC1187
Ultra-low cluster plate

Figure S4

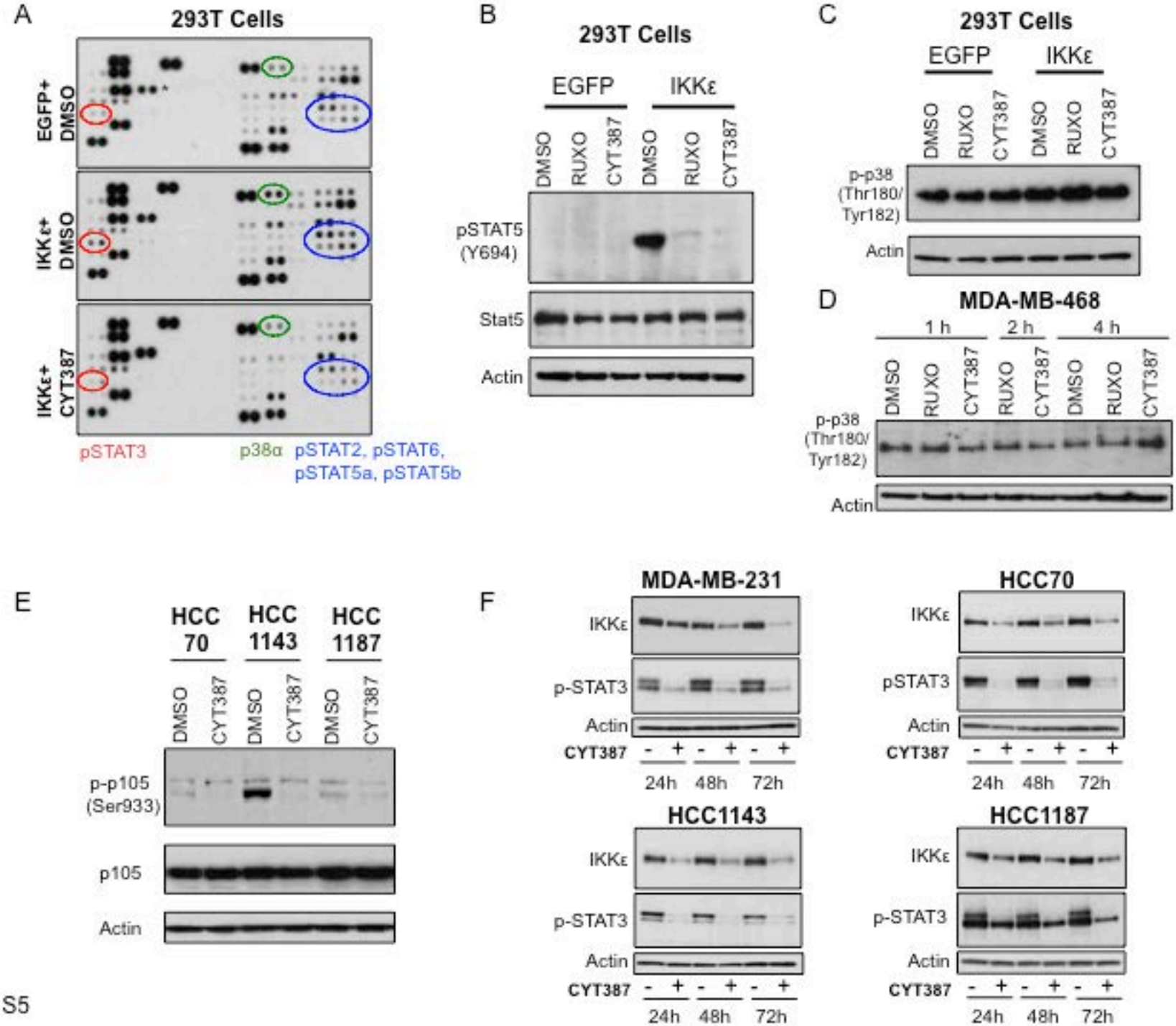
A
293T Cells
EGFP+ DMSO
IKKε+ DMSO
IKKε+ CYT387
pSTAT3
p38α
pSTAT2, pSTAT6, pSTAT5a, pSTAT5b
B
293T Cells
EGFP
IKKε
DMSO
RUXO
CYT387
pSTAT5 (Y694)
Stat5
Actin
C
293T Cells
EGFP
IKKε
DMSO
RUXO
CYT387
p-p38 (Thr180/ Tyr182)
Actin
D
MDA-MB-468
1 h
2 h
4 h
DMSO
RUXO
CYT387
p-p38 (Thr180/ Tyr182)
Actin
E
HCC 70
HCC 1143
HCC 1187
DMSO
CYT387
p-p105 (Ser933)
p105
Actin
F
MDA-MB-231
HCC70
HCC1143
HCC1187
IKKε
p-STAT3
pSTAT3
Actin
CYT387
- + - + - +
24h 48h 72h

Figure S5

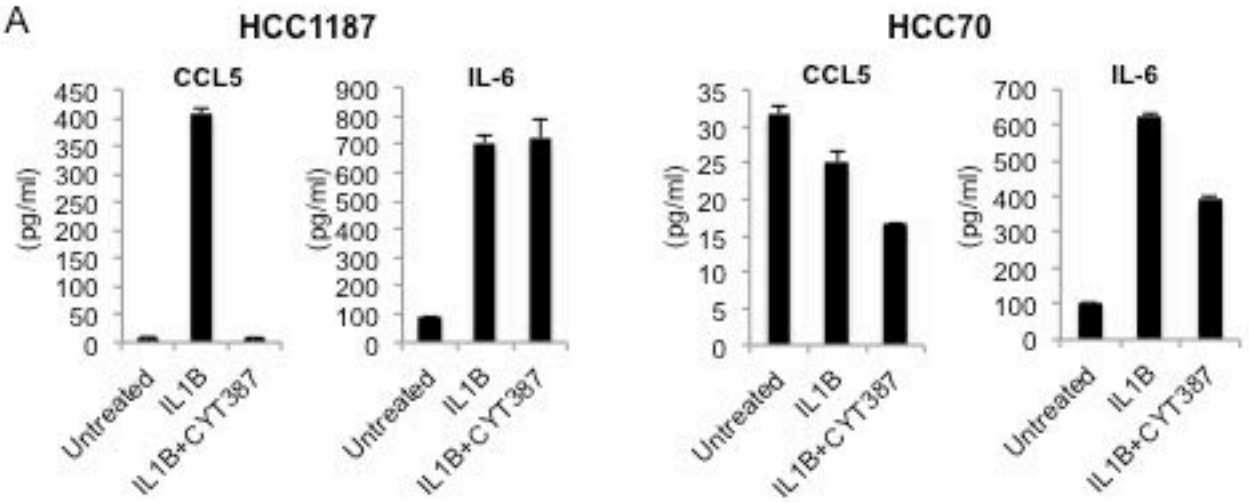
A
HCC1187
CCL5
IL-6
HCC70
CCL5
IL-6
(pg/ml)
Untreated
IL1B
IL1B+CYT387

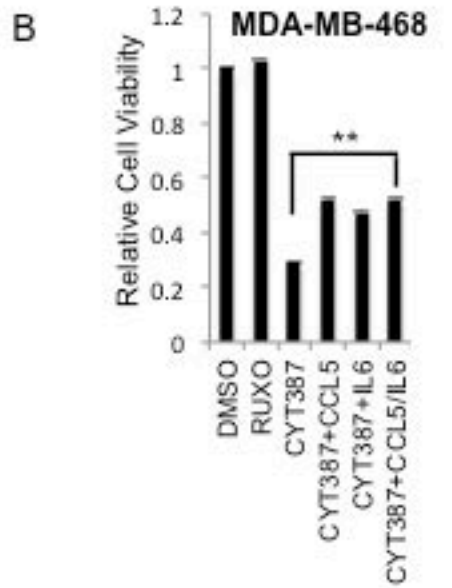
B
MDA-MB-468
Relative Cell Viability
**
DMSO
RUXO
CYT387
CYT387+CCL5
CYT387+IL6
CYT387+CCL5/IL6

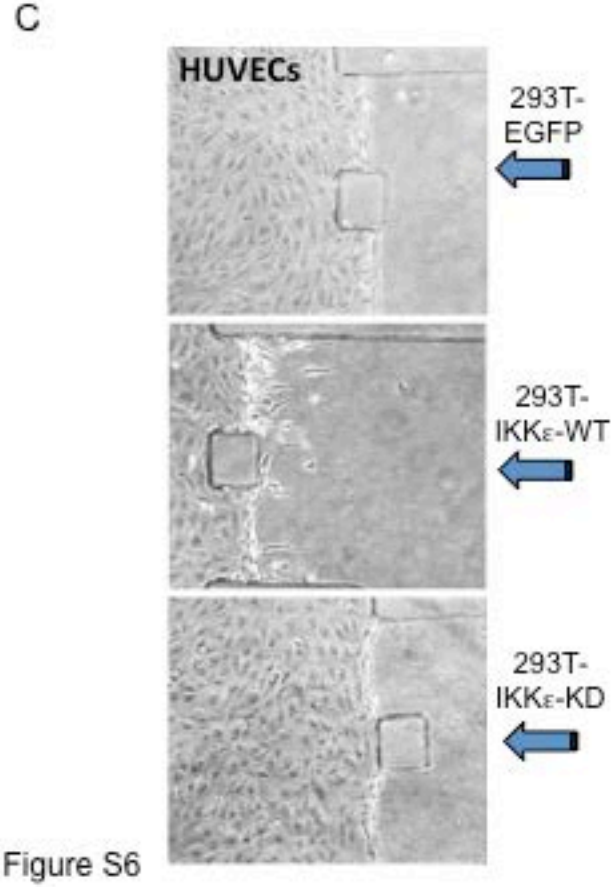
C
HUVECs
293T-EGFP
293T-IKKε-WT
293T-IKKε-KD

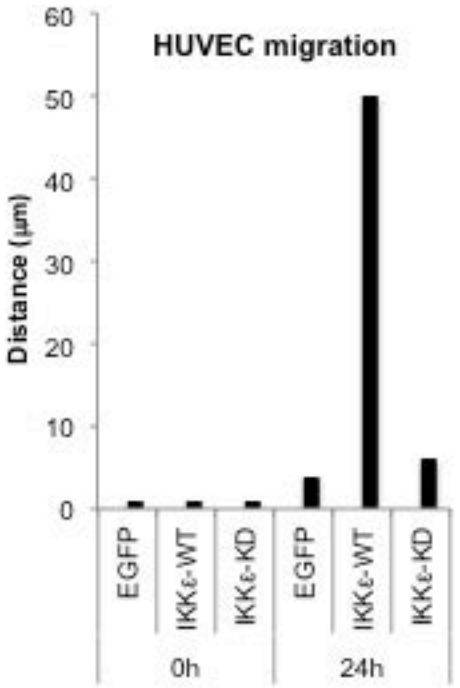
HUVEC migration
Distance (μm)
EGFP
IKKε-WT
IKKε-KD
0h
24h

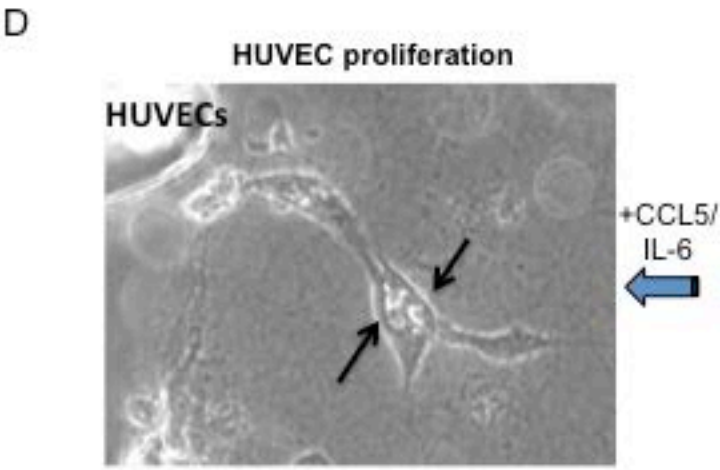
D
HUVEC proliferation
HUVECs
+CCL5/IL-6

Figure S6

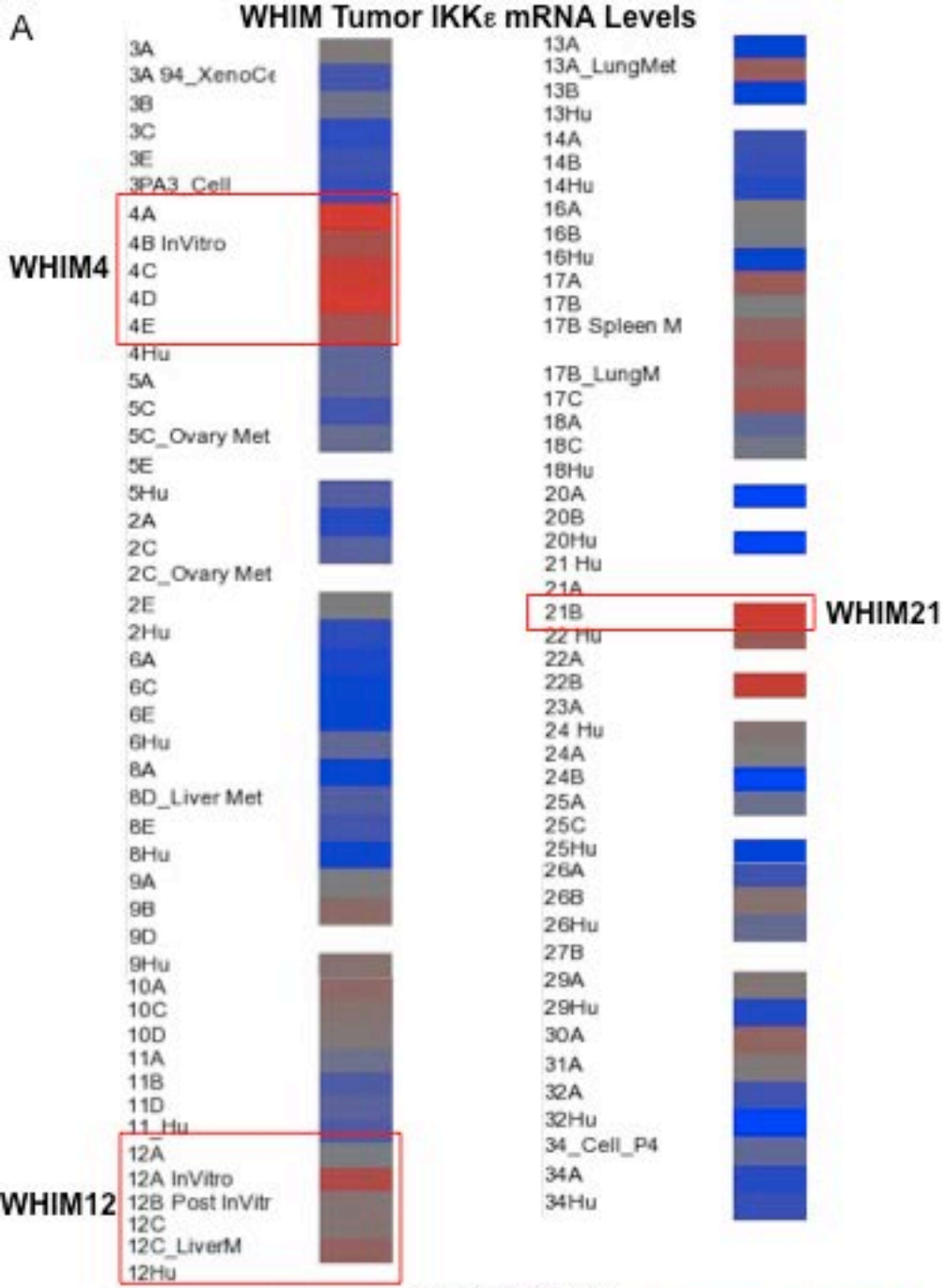
A
WHIM Tumor IKKε mRNA Levels
3A
3A 94_XenoCe
3B
3C
3E
3PA3_Cell
4A
4B InVitro
4C
4D
4E
4Hu
5A
5C
5C_Ovary Met
5E
5Hu
2A
2C
2C_Ovary Met
2E
2Hu
6A
6C
6E
6Hu
8A
8D_Liver Met
8E
8Hu
9A
9B
9D
9Hu
10A
10C
10D
11A
11B
11D
11_Hu
12A
12A InVitro
12B Post InVitr
12C
12C_LiverM
12Hu
13A
13A_LungMet
13B
13Hu
14A
14B
14Hu
16A
16B
16Hu
17A
17B
17B Spleen M
17B_LungM
17C
18A
18C
18Hu
20A
20B
20Hu
21 Hu
21A
21B
22 Hu
22A
22B
23A
24 Hu
24A
24B
25A
25C
25Hu
26A
26B
26Hu
27B
29A
29Hu
30A
31A
32A
32Hu
34_Cell_P4
34A
34Hu
WHIM4
WHIM21
WHIM12
Relative Expression
-2
0
+2

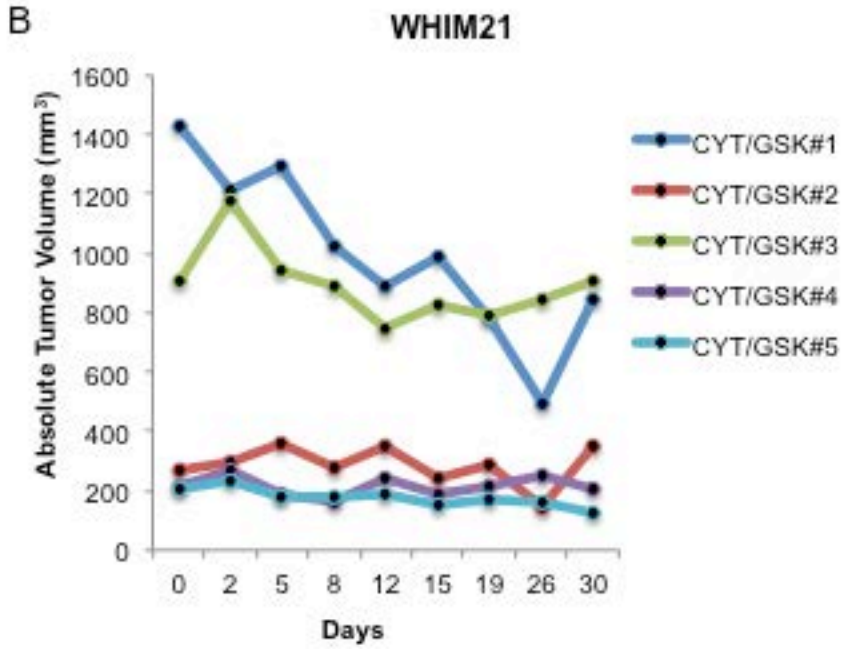
B
WHIM21
Absolute Tumor Volume (mm3)
1600
1400
1200
1000
800
600
400
200
0
0
2
5
8
12
15
19
26
30
Days
CYT/GSK#1
CYT/GSK#2
CYT/GSK#3
CYT/GSK#4
CYT/GSK#5

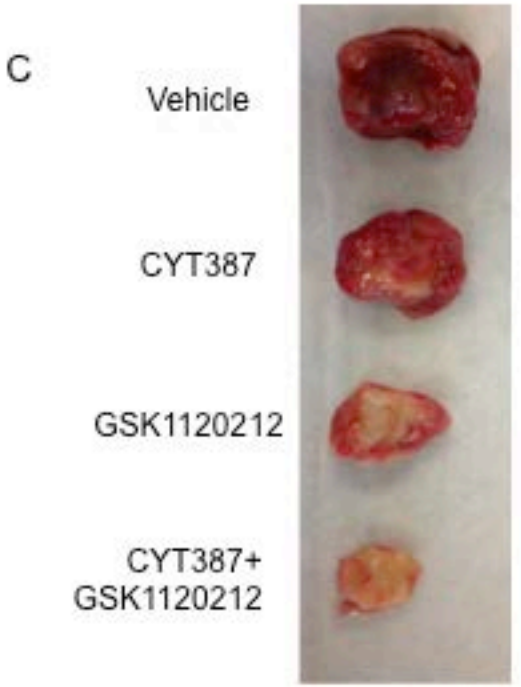
C
Vehicle
CYT387
GSK1120212
CYT387+
GSK1120212

Figure S7

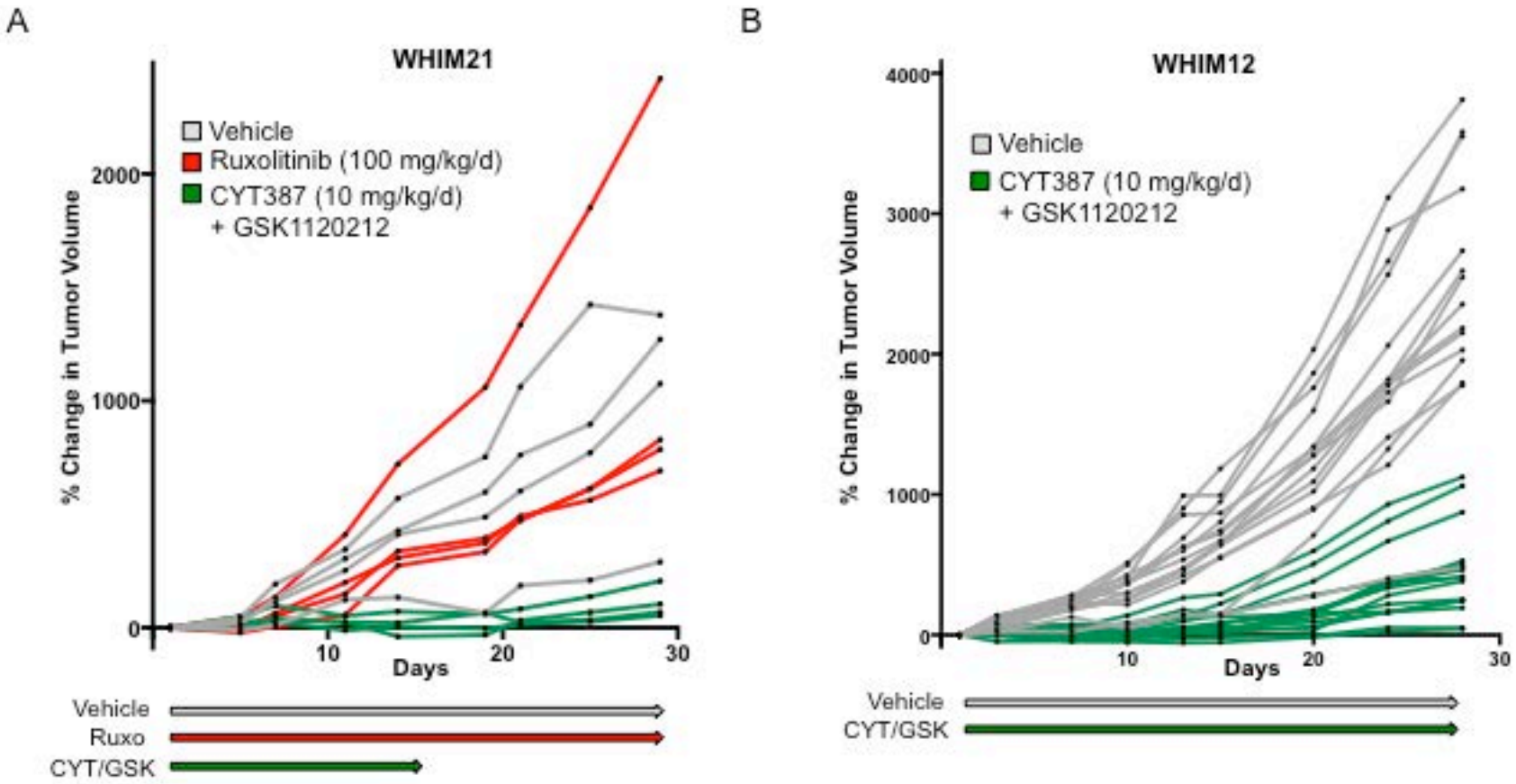
A
WHIM21
Vehicle
Ruxolitinib (100 mg/kg/d)
CYT387 (10 mg/kg/d)
+ GSK1120212
% Change in Tumor Volume
2000
1000
0
10
20
30
Days
Vehicle
Ruxo
CYT/GSK
B
WHIM12
Vehicle
CYT387 (10 mg/kg/d)
+ GSK1120212
% Change in Tumor Volume
4000
3000
2000
1000
0
10
20
30
Days
Vehicle
CYT/GSK

Figure S8

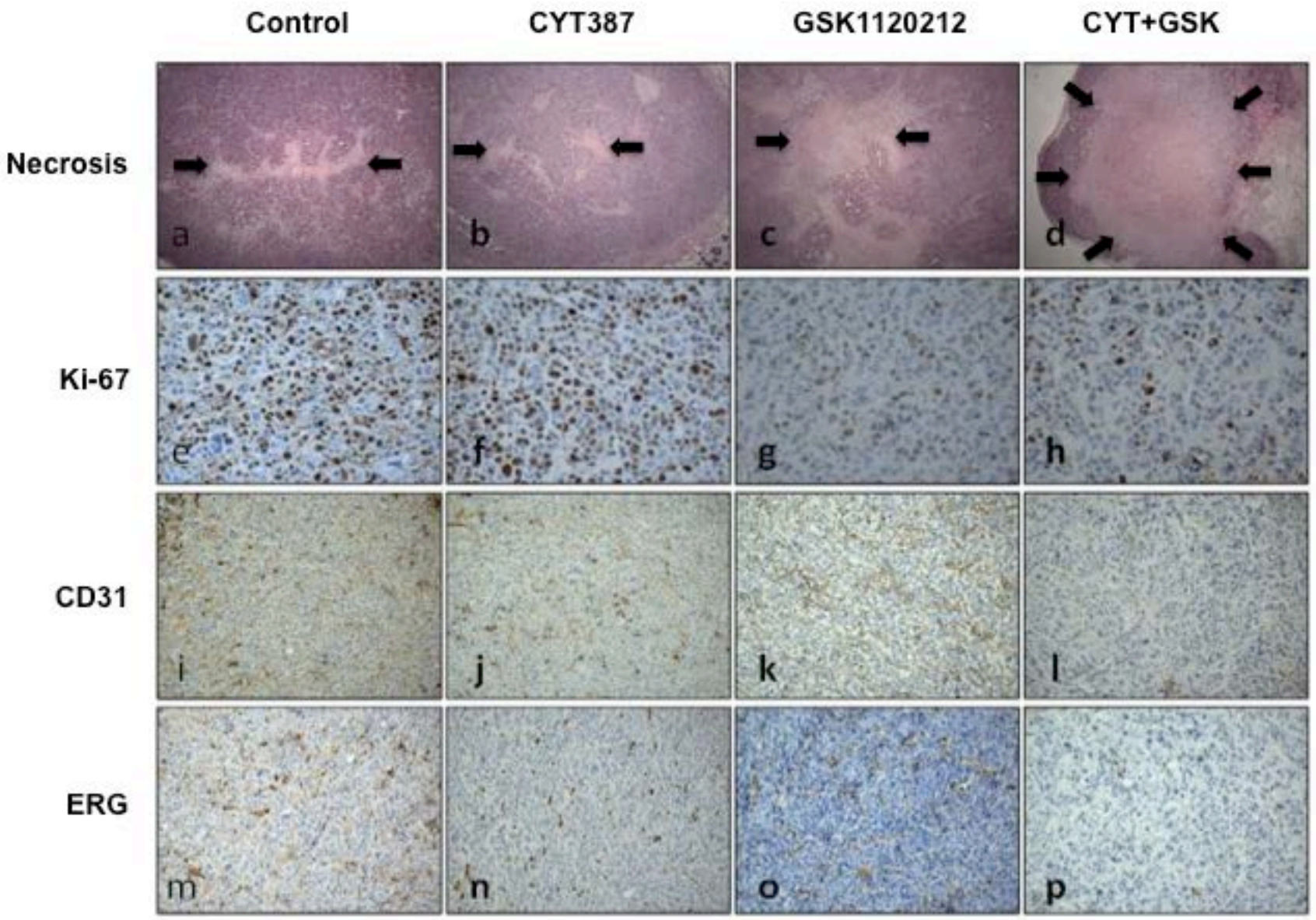
Control
CYT387
GSK1120212
CYT+GSK
Necrosis
Ki-67
CD31
ERG
a
b
c
d
e
f
g
h
i
j
k
l
m
n
o
p

Figure S9